RESEARCH ARTICLES

Radar Soundings of the Subsurface of Mars

Giovanni Picardi,[1] Jeffrey J. Plaut,[2]* Daniela Biccari,[1]
Ornella Bombaci,[3] Diego Calabrese,[3] Marco Cartacci,[1]
Andrea Cicchetti,[1] Stephen M. Clifford,[4] Peter Edenhofer,[5]
William M. Farrell,[6] Costanzo Federico,[7] Alessandro Frigeri,[7]
Donald A. Gurnett,[8] Tor Hagfors,[9] Essam Heggy,[4] Alain Herique,[10]
Richard L. Huff,[8] Anton B. Ivanov,[2] William T. K. Johnson,[2]
Rolando L. Jordan,[2] Donald L. Kirchner,[8] Wlodek Kofman,[10]
Carlton J. Leuschen,[11] Erling Nielsen,[9] Roberto Orosei,[12]
Elena Pettinelli,[14] Roger J. Phillips,[15] Dirk Plettemeier,[16]
Ali Safaeinili,[2] Roberto Seu,[1] Ellen R. Stofan,[17]
Giuliano Vannaroni,[13] Thomas R. Watters,[18] Enrico Zampolini[3]

The martian subsurface has been probed to kilometer depths by the Mars Advanced Radar for Subsurface and Ionospheric Sounding instrument aboard the Mars Express orbiter. Signals penetrate the polar layered deposits, probably imaging the base of the deposits. Data from the northern lowlands of Chryse Planitia have revealed a shallowly buried quasi-circular structure about 250 kilometers in diameter that is interpreted to be an impact basin. In addition, a planar reflector associated with the basin structure may indicate the presence of a low-loss deposit that is more than 1 kilometer thick.

The subsurface of Mars is unexplored territory. Glimpses of the third dimension of martian geology have been obtained by study of exposures on crater and valley walls (*1*) and by construction of cross sections inferred from geologic mapping of the surface (*2*, *3*). However, no direct measurements of the unexposed crust below a few meters depth were

possible before the activation of the Mars Advanced Radar for Subsurface and Ionospheric Sounding (MARSIS) (*4*) onboard the European Space Agency's Mars Express (*5*) orbiter in June 2005. We report here on radar echoes obtained by MARSIS from the deep subsurface, to more than 1 km depth.

The MARSIS instrument and data. MARSIS is a multifrequency, synthetic-aperture, orbital sounding radar. Data are collected when the elliptical orbit of Mars Express brings the spacecraft to an altitude of 250 to 800 km above the surface; this condition is met during about 26 min of each 6.7-hour orbit. In its subsurface modes, MARSIS operates in four frequency bands between 1.3 and 5.5 MHz, with a 1-MHz instantaneous bandwidth that provides free-space range resolution of approximately 150 m. Lateral spatial resolution depends on surface roughness characteristics, but for most Mars surfaces, the cross-track footprint is 10 to 30 km and the along-track footprint, narrowed by onboard synthetic-aperture processing, is 5 to 10 km. Peak transmitted power out of the 40-m dipole antenna is ~10 W. Coherent azimuth sums are performed onboard on ~100 pulses taken at a pulse repetition frequency of 127 Hz, with a resulting signal-to-noise ratio for a typical Mars surface of 30 to 50 dB. The data described here were acquired during the commissioning and initial routine data-collection phases of the MARSIS experiment, in June and July 2005. During this period, the close approach of the orbit occurred near the evening terminator.

MARSIS's sounding signals will not reach the surface when the ionospheric plasma frequency is close to or above the sounding frequency. The frequency bands were therefore chosen to minimize distortion by the ionosphere; typically, bands centered at 1.8 and 3.0 MHz were used on the nightside, and bands centered at 4.0 and 5.0 MHz were used on the dayside. Here we discuss data collected on orbits 1855, 1892, and 1903, on 26 June, 6 July, and 9 July 2005, respectively. Data were collected in a MARSIS subsurface-sounding mode, which returns complex spectra of summed pulses from three synthetic-aperture channels for each of two frequency bands. Once received on the ground, the spectra are transformed from the frequency domain to the time domain. Processing includes a correction for phase distortion in the ionosphere (*6*, *7*).

North polar layered deposits. Surrounding the north pole of Mars are the north polar layered deposits (NPLD) that consist mainly of an upper stratigraphic unit, thought to be dominated by water ice, which is typically finely layered because of varying fractions of included dust (*1*, *8–12*). A second, lower unit that is absent at some longitudes contains a substantial sand component that is probably ice-cemented (*10–12*). Previous compositional and stratigraphic interpretations of these deposits have been based on imaging, spectral, thermal, and topographic measurements. In an early MARSIS orbit, 1855, the NPLD were briefly observed in the longitude range from 10° to 40°E from altitudes of 800 to 900 km, on the nightside, in the frequency bands centered at 3.0 and 5.0 MHz. The radargrams show the surface reflection splitting into a pair of strong reflectors as the ground track passes from the northern plains onto the layered deposits (Fig. 1). The lower reflector extends to the end of the track, where it occurs at a time delay of 21 μs relative to the surface reflection. The interpretation of radar sounding data requires discriminating between signals arising from subsurface interfaces and those coming from surface topographic features at the same time delay (surface "clutter"). A high-fidelity model of the expected contribution of off-nadir topographic clutter, based on gridded Mars Orbiter Laser Altimeter (MOLA) data (*13–15*), shows no visible surface topographic feature that explains this reflector pair. Hence, we conclude that the second reflector is a subsurface ("basal") reflector.

The time delay to and the relative echo strength of the basal reflector are consistent with the overlying material (away from the boundary) having a dielectric constant and loss tangent (*16*) similar to that of fairly pure water ice. This is in accord with the absence of the lower, sandy stratigraphic unit in this region of the NPLD, as inferred from its lack of exposure in troughs in the longitude range from 290° to 90°E (*10*, *12*).

[1]Infocom Department, "La Sapienza" University of Rome, 00184 Rome, Italy. [2]Jet Propulsion Laboratory, California Institute of Technology, Pasadena, CA 91109, USA. [3]Alcatel Alenia Space Italia, 00131 Rome, Italy. [4]Lunar and Planetary Institute, Houston, TX 77058, USA. [5]Fakultaet fuer Elektrotechnik und Informationstechnik Ruhr-Universitaet Bochum, D-44780 Bochum, Germany. [6]NASA/Goddard Space Flight Center, Greenbelt, MD 20771, USA. [7]Dipartimento di Scienze della Terra, Università degli Studi di Perugia, 06123 Perugia, Italy. [8]Department of Physics and Astronomy, University of Iowa, Iowa City, IA 52242, USA. [9]Max Planck Institute for Solar System Research, 37191 Katlenburg-Lindau, Germany. [10]Laboratoire de Planetologie de Grenoble, 38041 Grenoble Cedex, France. [11]Applied Physics Laboratory, Johns Hopkins University, Laurel, MD 20723, USA. [12]Istituto di Astrofisica Spaziale e Fisica Cosmica, [13]Istituto di Fisica dello Spazio Interplanetario, Istituto Nazionale di Astrofisica, 00133 Rome, Italy. [14]Dipartimento di Fisica, University of Rome 3, 00146 Rome, Italy. [15]Department of Earth and Planetary Sciences, Washington University, St. Louis, MO 63130, USA. [16]Fakultaet fuer Elektrotechnik und Informationstechnik, Technische Universitaet Dresden, D-01062 Dresden, Germany. [17]Proxemy Research, Laytonsville, MD 20882, USA. [18]Center for Earth and Planetary Studies, National Air and Space Museum, Smithsonian Institution, Washington, DC 20560, USA.

*To whom correspondence should be addressed. E-mail: plaut@jpl.nasa.gov

The basal reflector time delay increases, with respect to the surrounding plains, as it proceeds inward from the NPLD boundary (Fig. 1). This is due to the slower velocity of the NPLD material relative to the martian atmosphere (approximately free-space velocity). Converting time to distance using a dielectric constant of pure ice (~3) brings the maximum basal reflector depth up to about the level of the plains; i.e., the depth to the reflector is approximately the height of the NPLD above its surroundings (about 1.8 km at the right edge in Fig. 1). Either this is a coincidence or the material in this region of the NPLD is dominated by ice sitting directly on the underlying plains material.

The wave attenuation properties strengthen the case for nearly pure ice. Among plausible geological materials, only pure or slightly dirty water ice has a sufficiently low value of loss tangent to explain the strength of the subsurface reflection observed. Simple two-layer modeling has been applied to estimate the loss tangent of the ~1.8-km NPLD layer. The two interfaces considered are one at the atmosphere/surface ice boundary and a second at the ice base at ~1.8-km depth. The MARSIS-measured ratio of the reflected power from these two interfaces at 5 MHz is approximately –10 dB. This ratio is consistent with an ice-layer dielectric of 3, an underlying material dielectric of 4.5 (basaltic regolith), and an ice-layer loss tangent that must be low, below 0.001 (conductivity $<10^{-6}$ siemens/m). The low loss tangent of the 1.8-km-thick ice layer gives rise to relatively low attenuation of MARSIS radar signals, thereby allowing the base to be easily detectable. Ice conductivity is temperature-dependent (17–19). The low loss and low conductivity of the ice indicate that it cannot contain more than a trace (2%) of impurities, and suggest a bulk temperature below 240 K. These observations are inconsistent with the presence of a melt zone at the base of the NPLD.

The NPLD will act as a load on the underlying elastic lithosphere and should cause a flexural/membrane downward deflection of the plains. In order to leave a residual deflection after the velocity conversion, the dielectric constant of the NPLD would have to be less than 3, which we deem unlikely. An elastic thickness in excess of 150 km would produce a deflection of 500 m or less (20), which is well within the resolution of our interface detection. Thus, a very thick elastic lithosphere (and a low crust/upper mantle temperature gradient) is implied for the north polar region.

Detection of ring structure. The midlatitude northern lowlands region known as Chryse Planitia (Fig. 2) has long been recognized as a locus of deposition of sediments delivered in outflow flooding events from multiple sources in the highlands (21–25). In image data and MOLA topography, the surface is characterized by textures ranging from smooth to hummocky, with numerous iso-
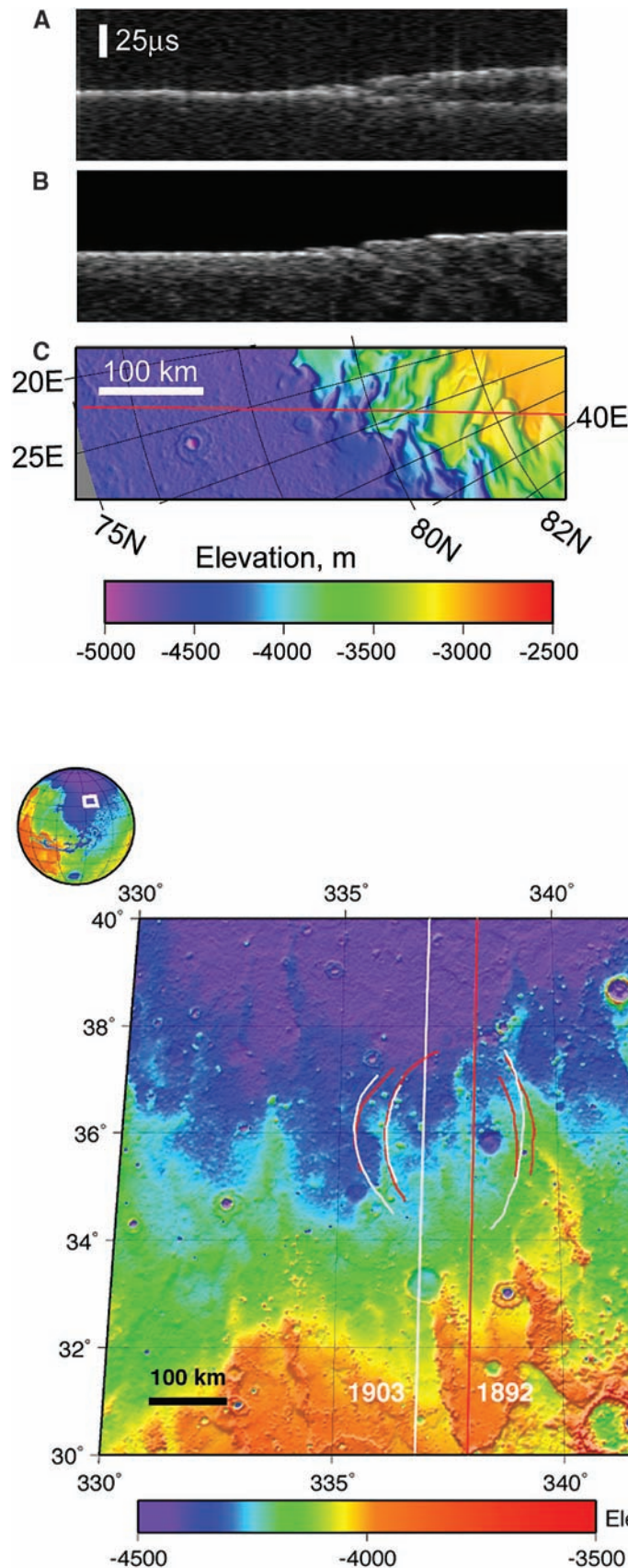

Fig. 1. (A) MARSIS data in radargram format for orbit 1855 as it crossed the margin of the NPLD. (B) Simulated MARSIS data if echoes are only from the surface (nadir and off-nadir clutter). (C) MOLA topography along the ground track (red line); elevation is relative to mean planetary radius. MARSIS data at 5 MHz show a split of the strong return into two as the ground track reaches the NPLD (higher terrain to the right). Maximum time delay to the second reflector is 21 µs, equivalent to 1.8-km depth in water ice.
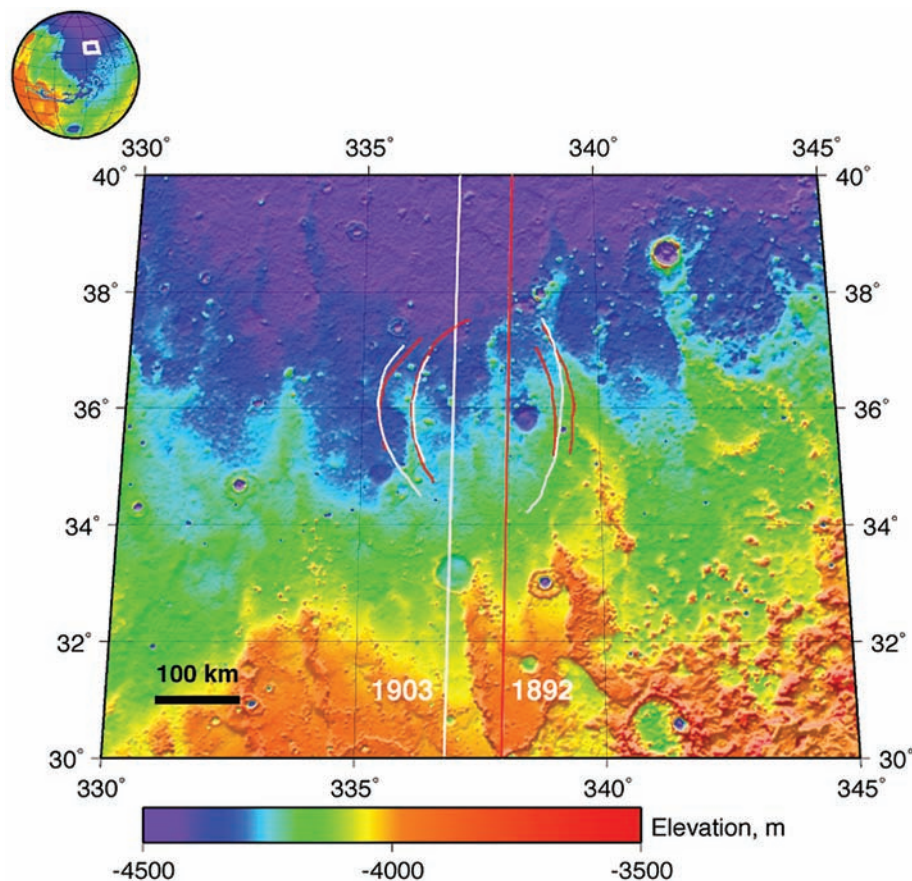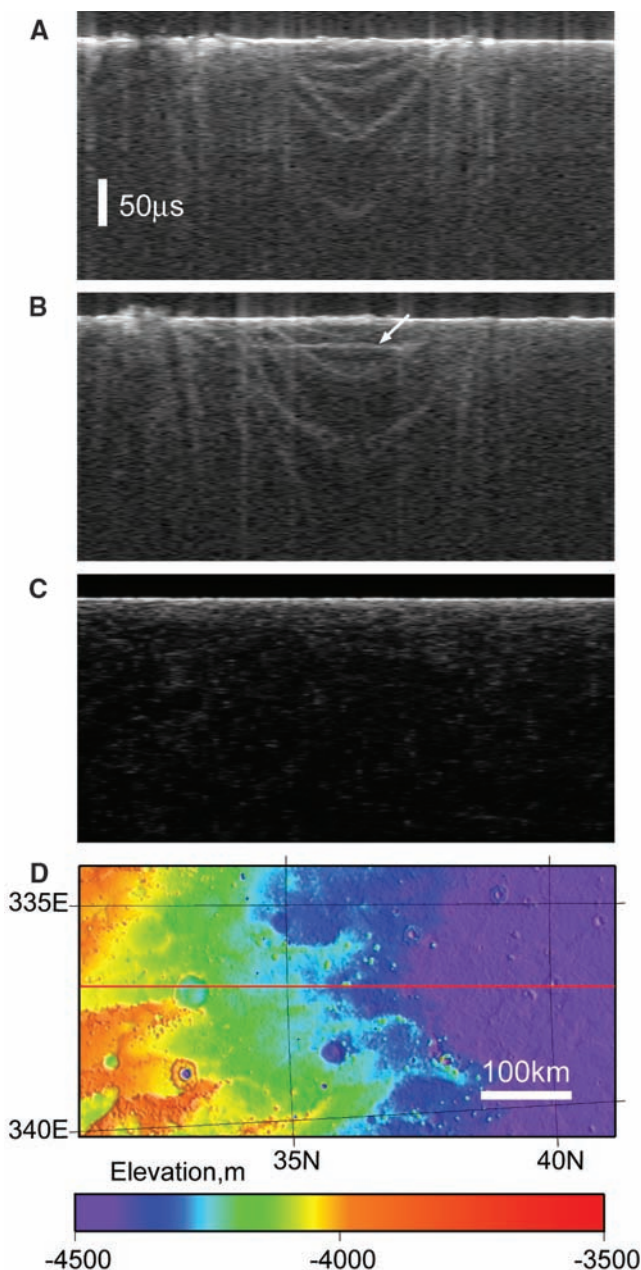

Fig. 2. Location of the ring structure, northeast Chryse Planitia, in MOLA topographic data (positive east longitude). The inset at top left shows the location of the detailed map on a globe of Mars. Ground track positions are shown as vertical lines (1903 and 1892). Traces of ring structures that match in the two orbits are shown in red (1892) and white (1903).

Fig. 3. MARSIS data for orbits (**A**) 1892 (3-MHz band) and (**B**) 1903 (4-MHz band). Note the multiple arc-shaped reflectors near the center of each panel, and the planar reflector associated with the arcs in orbit 1903 (arrow). (**C**) Model of the nadir surface and off-nadir clutter for orbit 1903. No arc-like or planar features are predicted in the clutter model. (**D**) MOLA topography along the ground track of orbit 1903.

at time delays later than the surface echo were seen in both orbits, centered at a common latitude of about 36°N (Fig. 3). The structures include multiple parabolic arcs in each orbit, with a common axis of symmetry and an additional planar reflector parallel to the surface trace, 160 km in length along-track, seen only in orbit 1903. The time delays of the arc features relative to the surface echo range from nearly coincident to delays up to 180 μs. Such long delayed echoes are not expected from the nadir subsurface at these frequencies, because they imply implausible penetration depths as great as 15 km. Rather, these echoes are likely a form of off-nadir clutter. The model of topographic clutter (Fig. 3), however, shows no features corresponding to the arcs or planar feature in these orbits. We therefore attribute the arc echoes to off-nadir clutter, but from a source below the surface.

The radargrams, which are in a time-delay geometry ("slant range") were transformed into a ground-range geometry, assuming that the detected features are at shallow depth. The ground-range projection transforms the parabolic echoes into arcs of constant curvature suggesting large circular features. Such a projection has a natural left/right ambiguity. The two orbit ground tracks are separated by about 50 km and provide a "stereo" viewing geometry. When the projected data are overlapped, some echoes from both orbits align (Fig. 2), suggesting that MARSIS imaged the same features twice and that the model of a near-surface structure is approximately correct. The matching arcs appear to trace out portions of several quasi-circular features. We interpret these rings as the rims of one or more buried impact basins, with a maximum diameter of ~250 km. A schematic representation of the detection of such a feature by a radar sounder is similar to the signature seen in the data (Fig. 4). We attribute the signature in the MARSIS data to reflections off of favorably oriented crater walls or related structures (such as rim-wall slump blocks or peak-ring features), where a contrast in electrical properties exists between the wall material and the basin fill or overlying materials. We note that no single circle or set of concentric circles exactly matches the ground range projection of the detected rings. This may be due to multiple overlapping structures, propagation effects not accounted for in the projection, or other unrecognized effects.

The planar reflector seen in orbit 1903 (Fig. 3) differs from the arc reflectors in several ways. First, it was seen at a remarkably uniform time delay from the surface echo (a mean delay of 29 μs, with a standard deviation of <2 μs in 26 measurements). Second, the intensity of the echo is significantly higher than that of the arcs, with a value of 16 ± 6 dB below the surface echo power in the same profiles. There is no obvious counterpart to this reflector in orbit 1892, although a subtle, shorter, early subhorizontal feature is observed that may be related. Here we explore the possibility that the feature in orbit

lated knobs, several subdued wrinkle ridges, and highly degraded or buried crater forms. In northeastern Chryse Planitia, surficial units of Late Hesperian and Early Amazonian age (based on crater counts) have been interpreted primarily as aqueous sediments, though some workers did not rule out an origin as lava flows (*26*). The area has been mapped recently as the "interior unit" of the Vastitas Borealis Formation (VBF), near its southern contact with Hesperian channeled plains material (*25*). The materials underlying the VBF that resurfaced Chryse Planitia and much of the ancient crust of the northern lowlands appear to be volcanic in origin, based on numerous partially buried wrinkle ridges similar to those found in exposed volcanic plains in the highlands (*27*). Using MOLA data, numerous large (tens

to hundreds of kilometers in diameter) subtle circular features were identified in the area (*28*, *29*) and were interpreted as surface expressions of a population of ancient degraded and/or buried impact craters. However, no structure corresponding to the feature described below has been identified previously.
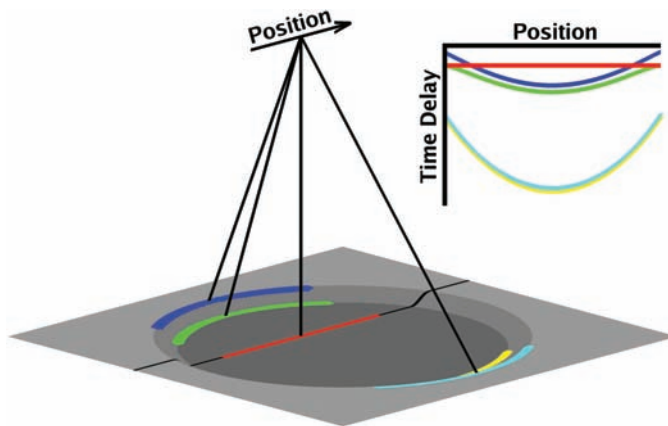
MARSIS observed part of the Chryse Planitia region on two orbits (1892 and 1903), at 30° to 40°N latitude, 330° to 340°E longitude, when the spacecraft altitude was ~335 km (near periapsis) and the solar zenith angle was within a few degrees of 90° [the terminator (Fig. 2)]. The higher frequency band for each dual-frequency observation obtained the best data, which for orbit 1892 was the band centered on 3 MHz and for orbit 1903 the band centered on 4 MHz. A distinctive collection of echo structures arriving

Fig. 4. Schematic showing the geometric relationships of a crater rim and floor in oblique view (**left**) and as seen in a sounder radargram (**right**). Note the appearance of multiple parabolic arcs and an associated planar reflector in the radargram. Compare with the radargram of orbit 1903 in Fig. 3.

1903 is a deep subsurface interface directly below the ground track of orbit 1903. This is consistent with the expected relationship of the geometric elements of a flat-floored circular basin when observed by a radar sounder (Fig. 4).

We again apply a simple two-layer model, in which the lower reflector occurs at the interface between a uniform upper layer and a lower layer of differing dielectric constant. The time delay translates to a depth to the interface of 2.0 to 2.5 km, for a plausible range of martian materials. The ratio of echo power between the two interfaces implies very low attenuation in the upper layer, with a loss tangent <0.005. This raises the intriguing possibility that a large volume of low-loss material, possibly ice-rich, at least partially fills the basin. The depth of the feature is roughly consistent with the observed depths of exposed 200- to 300-km-diameter basins on Mars. Thus, the feature could be the basin floor or a boundary between layers of basin fill. We cannot completely rule out the possibility that it is a ''hidden'' planar clutter structure that fortuitously lies almost exactly parallel to the orbital ground track. The putative interface extends ~160 km along-track, yet is not seen in the adjacent orbit 50 km to the east. Further observations are needed to understand this discrepancy. One possibility is that the eastern part of the basin floor was disrupted by a smaller, later impact event that formed a ~30-km-diameter crater (now degraded) that lies close to the ground track of orbit 1892 (Fig. 2). The ring feature and planar reflector occur near a crustal magnetic field anomaly (30). Our analysis does not show a major influence of the magnetic field on the radar signature, with the exception of some decorrelation (left side of Fig. 3) where there is a large gradient in the magnetic field (31).

Discussion and conclusions. MARSIS has demonstrated a capability to detect structures and layers in the subsurface of Mars that are not detectable by other sensors, past or present. In its only observation of the NPLD, the sounder has apparently penetrated >1 km of the ice-rich deposits, probably imaging the basal contact.

The low attenuation observed in the NPLDs indicates a composition of nearly pure cold water ice. The lack of a significant deflection of the plains surface below the NPLD implies a very thick elastic lithosphere in this region. In the mid-latitude Chryse Planitia, MARSIS has detected a circular structure ~250 km in diameter, presumably of impact origin. Embedded in this structure is a continuous reflector that may be the basin floor beneath a thick volume of low-loss material, although other explanations cannot be ruled out. Data described here from the first month of MARSIS observations indicate that the experiment holds promise to address a number of issues in Mars geology through subsurface probing. For example, if further observations of the polar layered deposits show comparable penetration to that seen in the example here, we can expect to map in detail the base of the layered deposits and to obtain better estimates of the deposits' volume. The detection of a large buried impact basin suggests that MARSIS data may be used to further expose the population of impact craters hidden beneath the surface in the northern lowlands and elsewhere on the planet.

References and Notes

1. M. C. Malin, K. S. Edgett, *J. Geophys. Res.* **106**, 23429 (2001).
2. D. H. Scott *et al.*, *U.S. Geol. Surv. Misc. Invest. Ser.*, Maps I-1802-A, -B, and -C (1987).
3. N. E. Witbeck *et al.*, *U.S. Geol. Surv. Misc. Invest. Ser.*, Map I-2010 (1991).
4. G. Picardi *et al.*, in *Mars Express: A European Mission to the Red Planet* [SP-1240, European Space Agency (ESA) Publications Division, European Space Research and Technology Centre (ESTEC), Noordwijk, Netherlands, 2004)], pp. 51–69.
5. A. Chicarro, P. Martin, R. Trautner, in *Mars Express: A European Mission to the Red Planet* (SP-1240, ESA Publications Division, ESTEC, Noordwijk, Netherlands, 2004), p. 313.
6. The ionosphere both attenuates the signal amplitude and scrambles its phase, resulting in defocusing of the radar echo return. The level of distortion depends on the electron content and collision frequency in the ionosphere, which in turn are related to the Sun elevation angle at the time of observation and the effects of solar activity on the martian plasma. Our ground processing includes a step that decodes the ionospheric phase distortion and refocuses the echo using redundant information in the data themselves and a priori information about local topography (7).
7. A. Safaeinili *et al.*, *Planet. Space Sci.* **51**, 505 (2003).
8. P. C. Thomas *et al.*, in *Mars*, H. H. Kieffer *et al.*, Eds. (Univ. of Arizona Press, Tucson, AZ, 1992), pp. 767–795.
9. E. Kolb, K. Tanaka, *Icarus* **154**, 22 (2001).
10. S. Byrne, B. C. Murray, *J. Geophys. Res.* **107**, 10.1029/2001JE001615 (2002).
11. K. S. Edgett *et al.*, *Geomorphology* **52**, 289 (2003).
12. K. E. Fishbaugh, J. W. Head III, *Icarus* **174**, 444 (2005).
13. D. E. Smith *et al.*, *Science* **284**, 1495 (1999).
14. MOLA topographic data at 1/128 degree per pixel grid spacing were used to simulate echoes from the cross-track region for each MARSIS subsurface sounding observation. Along-track sources were suppressed, because MARSIS data processing achieves this by aperture synthesis (15).
15. J.-F. Nouvel *et al.*, *Radio Sci.* **39**, 10.1029/2003RS002903 (2004).
16. We use the term "dielectric constant" to indicate the real part of the complex dielectric constant (relative permittivity) of a material ($\varepsilon = \varepsilon_r + i\varepsilon_i$), which is ratioed to the free-space value (r, real; i, imaginary). "Loss tangent" is the ratio $\varepsilon_i/\varepsilon_r$, or, equivalently, the ratio of electrical conductivity (s) to the product of angular frequency ($\omega = 2\pi f$) and ε_r.
17. D. C. Nunes, R. J. Phillips, in preparation.
18. W. M. Farrell *et al.*, *Geophys. Res. Lett.* **32**, L11204 (2005).
19. Y. Xu *et al.*, in preparation.
20. C. L. Johnson *et al.*, *Icarus* **144**, 313 (2000).
21. B. K. Lucchitta *et al.*, *Proc. Lunar Planet. Sci. Conf. 17th, Part 1*, *J. Geophys. Res.* **91**, E166 (1986).
22. S. Rotto, K. L. Tanaka, *U.S. Geol. Surv. Misc. Invest. Ser.*, Map I-2441 (1995).
23. K. L. Tanaka, *J. Geophys. Res.* **102**, 4131 (1997).
24. K. L. Tanaka *et al.*, *J. Geophys. Res.* **108**, 10.1029/2002JE001908 (2003).
25. K. L. Tanaka *et al.*, *U.S. Geol. Surv. Misc. Invest. Ser.*, Map I-2888 (2005).
26. G. E. McGill, *U.S. Geol. Surv. Misc. Invest. Ser.*, Map I-2811 (2005).
27. J. W. Head *et al.*, *J. Geophys. Res.* **107**, 10.1029/2000JE001445 (2002).
28. H. V. Frey *et al.*, *Geophys. Res. Lett.* **29**, 10.1029/2001GL013832 (2002).
29. H. V. Frey, *J. Geophys. Res.*, in press.
30. J. C. Cain *et al.*, *J. Geophys. Res.* **108**, 10.1029/2000JE001487 (2003).
31. The nearby magnetic anomaly has a peak magnitude of 310 nT (30). The depolarization of the radar wave due to the interaction of the magnetic field and ionosphere of Mars can cause ~1 μs of dispersion in the returned echo and cannot account for any of the features observed. Because the interaction of ionosphere with radar wave in the presence of a magnetic field is frequency-dependent, we plan to observe the feature in the future with different frequency bands.
32. MARSIS owes its existence to the funds and management of the Agenzia Spaziale Italiana (ASI) and NASA. The Mars Express mission is managed and operated by the European Space Agency. We thank the key instrument contractors, Alenia Spazio, University of Iowa, and Northrop Grumman Space Technology/Astro Aerospace, as well as the Mars Express flight team, whose efforts were instrumental in the successful deployment of the MARSIS antenna. We also thank S. Hensley, S. Madsen, E. Rodriguez, P. Rosen of the Jet Propulsion Laboratory for a technical review of the data used in this paper, and J. van Zyl for his contribution to the instrument concept. The research activities of the MARSIS principal investigator and Italian investigators are supported by grants under the Mars Express/ASI program. Work of the U.S. investigators is supported by grants under the Mars Express/NASA project. Some of the research described in this publication was carried out at the Jet Propulsion Laboratory, California Institute of Technology, under a contract with NASA.